Chapter 15

Unlabeled Semen Analysis by Means of the Holographic Imaging

Giuseppe Coppola, Maria Antonietta Ferrara, Giuseppe Di Caprio, Gianfranco Coppola and Brian Dale

Additional information is available at the end of the chapter

http://dx.doi.org/10.5772/67552

Abstract

The morphology, the motility, and the biochemical structure of the spermatozoon have often been correlated with the outcome of *in vitro* fertilization and have been shown to be the sole parameters of the semen analysis in predicting the success of intracytoplasmic sperm injection and intracytoplasmic morphologically selected sperm injection. In this context, digital holography has demonstrated to be an attractive technique to perform a label-free, noninvasive, and high-resolution technique for characterization of live spermatozoa. The aim of this chapter is to summarize the recent achievements of digital holography in order to show its high potentiality as an efficient method for healthy and fertile sperm cell selection, without injuring the specimen and to explore new possible applications of digital holography in this field.

Keywords: holographic imaging, label-free techniques, human sperm structure, *in vitro* fertilization

1. Introduction

Following the advent of human *in vitro* fertilization [1], much attention has been given to understand both the spermatozoa morphological alterations and the kinematics/dynamics of the swimming spermatozoa [2–11]. In fact, semen analysis is commonly employed both in human and in the zoo-technic field. In the first case, the analysis is mainly applied to study the couple's infertility or to confirm success of male sterilization procedures. Moreover, several studies have shown that for infertile men, the risk for developing a testicular cancer is slightly higher-than-average. So, independently of the will to have children, male fertility is a good

indicator for general health. On the other hand, in the zoo-technic field, animal semen analysis is commonly used in animal production laboratories and reproductive toxicology.

The main requirements for the development of techniques used for an accurate semen analysis are the following:

- avoid any alteration of the health of the spermatozoa under test;
- use a label-free approach to eliminate all adverse effects of the probe labeling;
- obtain results independent on the technician's experience and/or the laboratory environmental conditions (such as temperature, humidity, and duration).

The sperm cell is almost transparent in conventional bright field microscopy, as its optical proprieties differ slightly from the surrounding liquid, generating little contrast. On the other hand, a light beam that passes through a spermatozoon undergoes a phase change, in comparison with the surrounding medium, the amplitude of which depends on the light source, the thickness, and the integral refractive index of the object itself. A qualitative visualization of this phase contrast may be obtained by contrast interference microscopy (phase contrast or Nomarski/Zernicke interferential contrast microscopy). However, it is difficult and time-consuming to obtain a quantitative morphological imaging. In fact, a fine z-movement of the biological sample is required in order to acquire a collection of different planes in focus. This collection of acquired images is used in postelaboration to produce a 3D image of the object under investigation [12]. The same approach has been used to obtain information about sperm motility. Nevertheless, this 2D intrinsic analysis implies a partial in-plane representation of the motility features due to difficulty to track the 3D spatial motion of spermatozoa that quickly move out of focus. In order to overcome these intrinsic limitations, several approaches have been recently developed. In this contest, the optical approaches are deeply investigated.

In particular, over the last few years, holographic imaging in microscopy has been established as a valid noninvasive, quantitative, label-free, high-resolution, and phase-contrast imaging technique. So this chapter tries to summarize the state-of-art on the semen analysis and recent achievements obtained by a holographic imaging [13–17]. We will show that the unique potentialities of the holographic imaging have been used to provide structural information on both the morphology and the motility of sperm cells [18]. Moreover, the combination of the holographic technique with others approaches, such as the Raman spectroscopy, will be described, too. In fact, spermatozoa from infertile men could present a variety of alterations (such as alterations of chromatin organization [19], aneuploidy [20], and DNA fragmentation [21]) that can decrease reproductive capacity of men. Current methods of DNA assessment are mainly based on fluorescence microscopy, and thus samples are unusable after the analysis [22–25]. Therefore, the ability to simultaneously analyze, in a nondestructive and noninvasive way, both the morphology and biochemical functionalities of the spermatozoa could bring greater understandings [26]. Thus, the chapter will allow a bird's-eye view into the potentiality of the semen analysis performed by means of the holographic imaging, showing that this approach is extremely important for the intracytoplasmic sperm injection (ICSI) procedure, where it is highly required the development of a method that allows characterizing and directly select the best spermatozoon to inject into the oocytes [9, 27].

http://dx.doi.org/10.5772/67552

2. Principle of the holographic imaging

An optical field consists of amplitude and phase distributions; if this field interacts with the object under test, the morphology of the object alters the phase distribution. The holographic approach employs the interference between two optical beams to transform the phase information (i.e., the morphological information) into a recordable intensity distribution [28]. A sketch of an experimental set up for holographic imaging is shown in **Figure 1**. It consists in a coherent laser beam splits into a reference and an object beam.

The object beam intensity is always set well below the level for causing any damage to the spermatozoa structure and functionality. A microscope objective lens is used to collect the object beam. The reference and the object beam are then recombined by a beam splitter onto a CCD (Charge-Coupled Device) or CMOS (Complementary Metal-Oxide Semiconductor) detector, which acquires the interference pattern. According to the angle θ between the reference and object beams, either on-axis ($\theta = 0°$) or off-axis configuration can be adopted. Besides, the hologram of the sample under investigation, a second hologram is acquired on a reference surface in proximity to the object in order to numerically compensate all the aberrations introduced by the optical components, including the defocusing due to the microscope objective. The image reconstruction

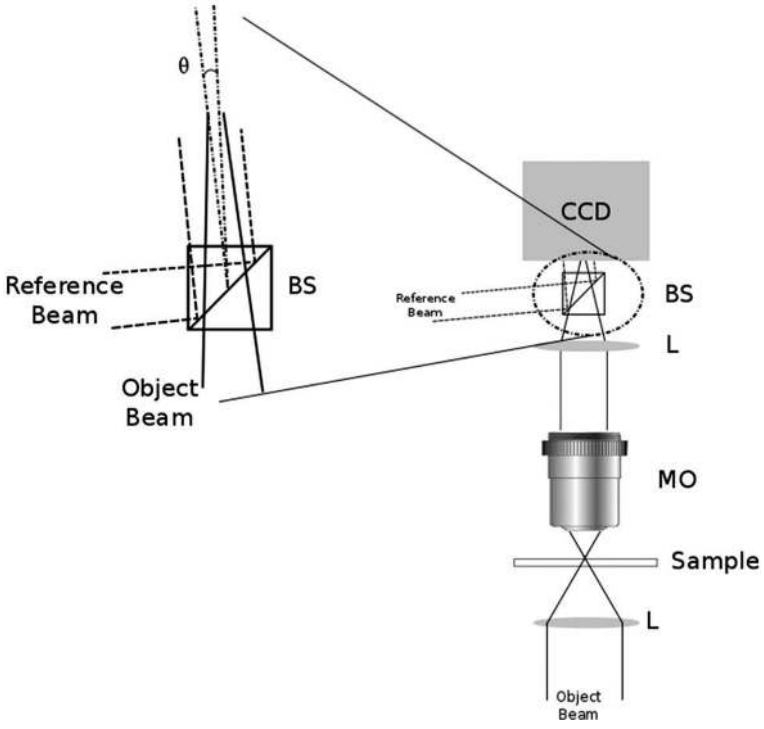

Figure 1. Sketch of the principle of hologram formation (L: lens, MO: microscope objective, BS: beam splitter).

procedure allows retrieving a discrete version of the complex optical wavefront (amplitude and phase) present on the surface of the specimen under test. This optical wavefront is obtained multiplying the recorded hologram by a numerical replica of the reference beam and numerically back-propagating this product. Actually, this product generates three diffraction terms: zeroth order, real image, and conjugate image. In an on-axis configuration, unless a partially coherent light is adopted that allows reducing the speckle and multi-reflection interference noise [29], all terms are superimposed. Thus, in order to recover only the real image, i.e., an exact replica of the object wavefront, either a spatial or temporal phase-shifting methods has to be employed. However, in this way the complexity and capture time increase [13]. On the other hand, by introducing a small angle between the object and reference beam (off-axis configuration), a spatial separation between the three terms is obtained, at the expense of suboptimal use of camera sensor space-bandwidth product. Thus, this separation allows selecting and retrieving only the real image. The possibility offered by DH to numerically retrieve the phase distribution of the object wavefront allows not only the possibility to evaluate the object morphology but also to remove and/or compensate the unwanted wavefront variation (such as optical aberrations and slide deformations) [30–32].

3. Morphological imaging

Coppola's group [33] investigated the possibility to better understand the sperm behavior by means of a quantitative analysis of the 3D spermatozoa's morphology. In particular, experiments on bovine sperm cells were performed. The recorded hologram is illustrated in **Figure 2**, whereas the intensity of the fringe pattern generated by the interference between the object and reference beam is highlighted into the inset.

In **Figure 3**, the reconstructed images of abnormal bovine spermatozoa are reported [33]. For the reported analysis, the spermatozoa were fixed and without the surrounding liquid. In particular, the retrieved image shown in **Figure 3(a)** is relative to a spermatozoon with a cytoplasmatic droplet along the tail. Cytoplasm surrounding the sperm cell is accumulated during maturation, and it is extruded from the cell in the last phases of this maturation. However, cytoplasmatic residues may persist in the cell and, in particular, are retained in the tail as a droplet [34]. Thus, the presence of drops along the tail is connected to the degree of cell maturation and may indicate an excessive utilization of a donor.

In **Figure 3(b)**, an image of a spermatozoon with a bent tail is shown. Generally, when this defect is present in the semen either before or after the freezing process, the donor may be afflicted with a reproductive problem. On the other hand, if this anomaly appears with high frequency only in frozen semen, it can indicate that the spermatozoa have been subjected to hypoosmotic stress possibly due to an improper use of freezing extender and to an extremely low concentration of solutes. Finally, the reconstructed image of a spermatozoon with broken acrosome is illustrated in **Figure 3(c)**. In particular, the loss of acrosomal substances indicates premature acrosome activation far from the site of fertilization. This defect is present with high percentage in frozen semen samples due to incorrect sperm handling during the freezing process. The great advantage of managing quantitative information allows carrying out different numerical analysis, such as estimation area/volume, profiles along particular

http://dx.doi.org/10.5772/67552

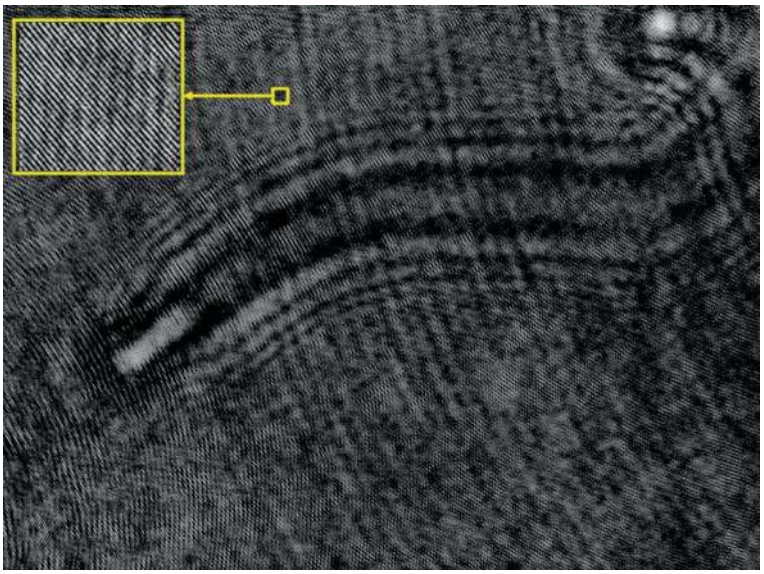

Figure 2. Acquired hologram, a region is enhanced in order to show the interference pattern (inset). Ref. [33] (by permission of IEEE Society).

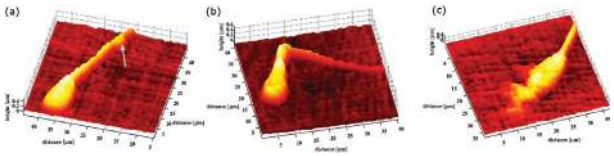

Figure 3. Pseudo 3D representation of the thickness of a spermatozoon with: (a) a cytoplasmatic droplet along the tail; (b) a bent tail; (c) an acrosome broken. Ref. [33] (by permission of IEEE Society).

directions, and selection of different zones. The 3D analysis can add further information to the data provided by the traditional bi-dimensional optical techniques, allowing to better understand the relationship between the male infertility and the abnormal morphology. Due to this potentiality, the holographic approach has been also employed to analyze the human sperm characteristics [35, 36]. Crha et al. [35] tested about 3000 sperm cells to individuate a phase difference between spermatozoa in normo-zoospermia (NZ) and oligoasthenoteratozoospermia (OAT). **Table 1** summarizes the obtained results in terms of mean, median, standard deviation (SD), and confidence intervals (CI).

The Dale's group performed a comparison between the results of spermatozoa analyzed both by a semiautomated digitally enhanced Nomarski microscopy (DESA) and by the holographic imaging [36]. In **Table 2**, the values relative to five primary parameters (length, width, perimeter, area, and volume) for normal human spermatozoa are compared. Results shows that no significant differences were observed in the gross morphometric values of the sperm cells analyzed.

Sperm group	Median	Mean	SD	CI
NZ	2.90	2.91	0.61	2.94
OAT	2.00	2.10	0.38	2.13

Table 1. Descriptive statistics for statistically significant ($\rho < 0.001$) phase shifts according to the NZ/OAT group [35].

Imaging	Length [μm]	Width [μm]	Perimeter [μm]	Area [μm^2]	Volume [μm^3]
DESA	5.1 ± 0.6	3.5 ± 0.4	13.8 ± 1.4	14.1 ± 2.0	-
Holography	5.6 ± 0.3	2.9 ± 0.5	14.3 ± 1.2	13.0 ± 1.2	8.0 ± 0.8

Table 2. Mean morphometric values of normal human sperm heads obtained by DESA and holographic techniques [36].

It is important to note that the volume estimation could not be performed by the DESA technique. Due the great influence of nuclear vacuoles in the sperm head on the fertilization capacitance of sperm cell [9], the volumetric analysis was performed to analyze vacuolated human spermatozoa. In **Figure 4(a)**, a conventional differential interference contrast (DIC) image of a vacuolated human sperm is reported. The holographic 3D reconstruction of the vacuolated spermatozoon is illustrated in **Figure 4(b)**. From this figure, it is clear that spermatozoa with vacuole had a reduced volume, and this reduction could be probably be due to variation of the inner structure of the sperm head with a loss of material.

Table 3 summarizes the volumetric analysis carried out for three different groups of spermatozoa defined by the length and width of the head. Mean values of the total volume of the spermatozoa minus the vacuoles volume are also reported.

Memmolo et al. [37] proposed to use DH in order to identify and measure specific region-of-interest of spermatozoa. **Figure 5** shows some steps of the applied method that starts from a filtered version of the reconstructed spermatozoon image and is able to identify the head region.

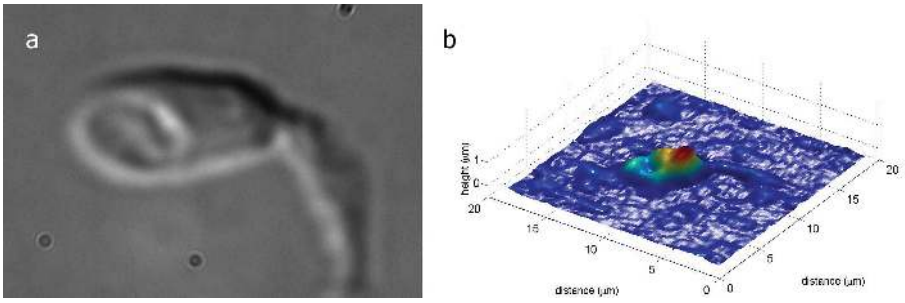

Figure 4. Differential interference contrast image (a) and pseudo 3D holographic reconstruction (b) of a vacuolated sperm head. Ref [36] (by permission of Cambridge University Press).

Sperm dimensions	Volume [μm³]	
	Total	Total vacuoles
Length < 2.9 μm, width < 4.2 μm	5.8 ± 0.7	4.0 ± 0.8
2.9 < length < 3.7μm; 4.2 < width < 5.3 μm	8.2 ± 0.8	6.4 ± 0.8
Length > 3.7 μm, width > 5.3μm	10.1 ± 0.8	8.4 ± 0.8

Table 3. Mean volumetric values of vacuolated sperm clustered in three different subpopulations [36].

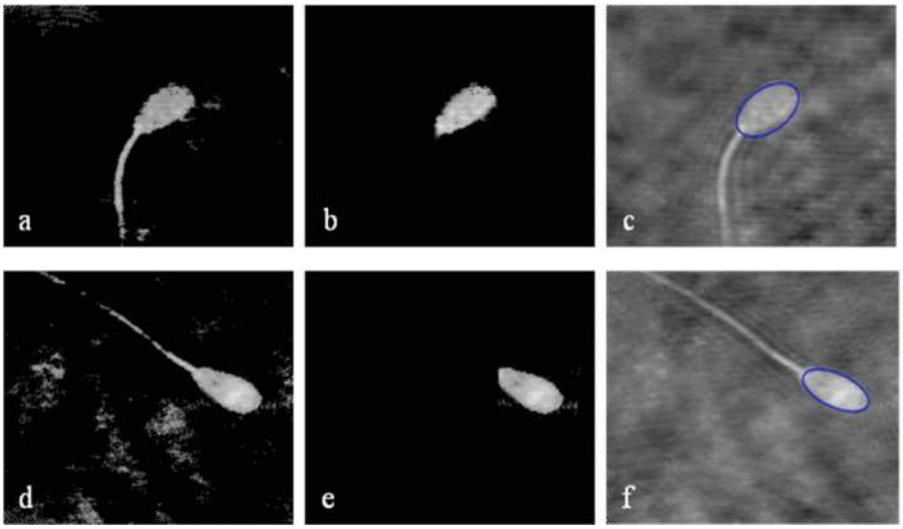

Figure 5. Detection of sperm head by the algorithm proposed by Memmolo et al. [37] (by permission of The Optical Society): (a) and (d) are the results of the denoising, (b) and (e) are the results of extraction algorithm, (c) and (f) are the best fit ellipses.

The proposed algorithm could be very useful to retrieve noisy holograms due to the impurity of the liquid surrounding the spermatozoa.

4. Tracking analysis

One of the main advantages of the holographic approach is the possibility to retrieve a quantitative 3D image by means of a numerical refocusing of only one bi-dimensional image at different object planes. Thus, the realigning of the optical imaging system with mechanical translation can be eliminated. This peculiarity enables the characterization of live specimen [38], and in particular, to track the 3D spatial motion of spermatozoa that quickly move out of focus. The tracking approach allows estimating many quantitative parameters useful for a semen analysis [39], such as:

- curvilinear velocity (VCL), i.e., the total distance that the sperm head covers in the observation period;
- straight-line velocity (VSL), i.e., determined from the straight-line distance between the first and last points of the trajectory and gives the net space gain in the observation period;
- average path velocity (VAP), i.e., the distance the spermatozoon has traveled in the average direction of movement in the observation period;
- linearity (LIN): a comparison of the straight-line and curvilinear paths;
- wobble (WOB): a comparison of the average and curvilinear paths; and
- amplitude of lateral head displacement (ALH).

However, traditional techniques provide all these data as in-plane parameters. Conversely, the holographic approach allows adding 3D information about the trajectory followed by the sperm cells in a volume. This additional information can provide a better understanding of the sperm behavior and its relation with male infertility [40]. The 3D trajectories of human sperms across a large volume have been dynamically tracked by the Ozcan's group using a lens-free holographic approach [41]. The employed method generates the hologram by the interference of two components of the same light beam (in-line configuration). In particular, the holographic setup is composed of two partially coherent light-emitting-diodes (LEDs) at two different wavelengths that illuminate the sperms vertically (red wavelength) and obliquely at 45° (blue wavelength) [41]. The combination of these two different images allows determining the 3D location of each sperm. In **Figure 6**, the 3D dynamic swimming patterns of human sperm evaluated by means of this approach are illustrated. In particular, the volume investigated was relative to a depth-of-field of about 0.5–1 mm and a field-of-view of >17 mm^2. The results show that most part of sperm (90%) moves forward swiftly along a slightly curved axis. The remaining part of spermatozoa exhibit a helical trajectory with a noticeable movement along the *z*-axis (about 4–5%) or a hyperactivated 3D swimming with large lateral movements (<3%) or a hyperhelical pattern (about 0.5%).

By means of the observation of these trajectories on a large number of sperm cells (>1500), a statistic analysis on various parameters has been estimated; in particular, in **Table 4** some of these parameters are summarized.

Furthermore, thanks to the high accuracy of the technique, the authors observed that among the helical human sperms, a significant majority (approximately 90%) preferred right-handed helices over left-handed ones, with a helix radius of approximately 0.5–3 μm.

A different approach has been proposed by Di Caprio et al. [42]. In particular, the authors used an off-axis set-up and the capabilities of holographic technique to retrieve in-focus images independently of the focal plane of the acquire image. Thus, in order to estimate the swimming trajectories of human sperm, a set of holograms was recorded, keeping constant the distance between the sample and the microscope objective. Each retrieved image is used to evaluate the *X* and *Y* coordinates of sperm cells, whereas to obtain the *Z* position,

http://dx.doi.org/10.5772/67552

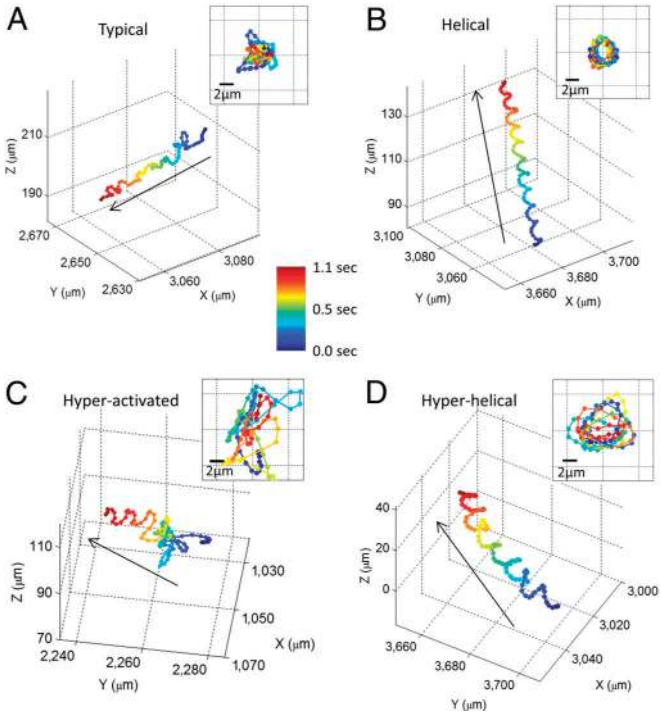

Figure 6. Swimming trajectories of human sperms evaluated by Ozcan's group Ref. [41] (by permission of the National Academy of Sciences). (A) The typical pattern. (B) The helical pattern. (C) The hyperactivated pattern. (D) The hyperhelical pattern. The inset in each panel represents the front view of the straightened trajectory of the sperm.

	VCL [μm/s]	VSL [μm/s]	Linearity [μm/μm]	ALH [μm]
Mean value	88.0 ± 28.7	55.7 ± 24.9	0.61 ± 0.21	5.4 ± 2.9

Table 4. Mean values of some parameters related to the motility of human sperm: curvilinear velocity (VCL), straight-line velocity (VSL), linearity, amplitude of lateral head displacement (ALH) [41].

a numerical self-focusing function was applied on the reconstructed images [43–45]. It is worth noting that the possibility to keep constant the distance sample-objective, allows an *in vitro* volumetric field reconstruction, i.e., not possible with the traditional optical techniques. Authors applied this approach to estimate the swimming pattern of a spermatozoon with a bent tail. As shown in **Figure 7**, this morphological anomaly causes a nonlinear out-of-plane motion.

Moreover, the authors reported the simultaneous tracking of five human spermatozoa, moving on a different focal plane (**Figure 8**). From the trajectories displayed in **Figure 8**, an anomalous one can be recognized (indicated by an arrow). In fact, while every other cell moves in parallel, the anomalous spermatozoon swims along a broken track and on a tilted direction.

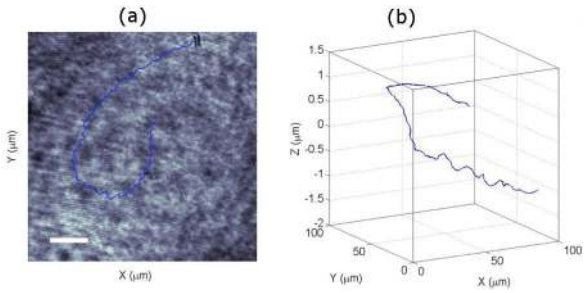

Figure 7. Transversal (a) and 3D path (b) of a sperm cell presenting a bent tail Ref. [42] (by permission of The Optical Society).

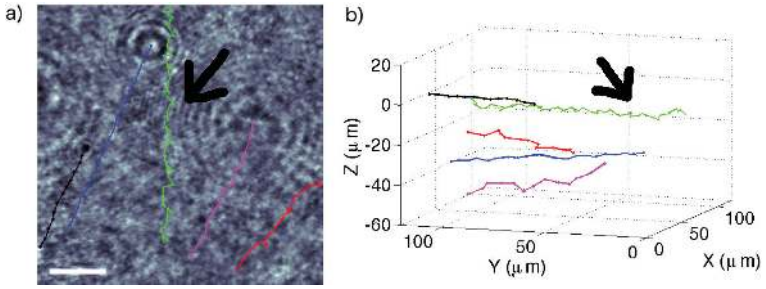

Figure 8. Multiple sperm cells tracking. Transversal (a) and reconstructed 3D path (b). Scale bar is 20 μm, data were acquired each 11 s. Ref. [42] (by permission of The Optical Society).

This anomalous behavior has been also confirmed by the retrieved motility parameters. In fact, the VSL measured for cell 1 (green) was about 10 μ/s, i.e., a value lower than those relating to other four cells (VSL_{mean} = 20 μ/s) and describes effectively the inefficient cell movement. Moreover, the "normal" cells (cells 2, 3, 4 and 5) have a reduced oscillation around the average path; in fact, their wobble is pretty uniform around 0.97 and 0.99. On the other hand, this value is sensibly lower for the "abnormal" cell, providing a quantitative description of the wide fluctuation of the spermatozoon head.

5. Combined approaches

A recent improvement in DH technique was proposed by Coppola's group combining DH with Raman spectroscopy [26]. This combined approach allows to simultaneously study biochemical and morphological characteristics of human sperm cells irradiated with green laser radiation. The scheme of the combined phase imaging interferometer and Raman microscope system is illustrated in **Figure 9**.

http://dx.doi.org/10.5772/67552

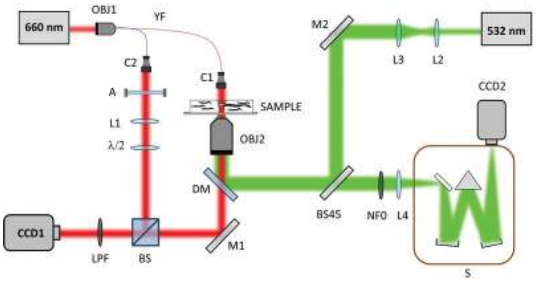

Figure 9. Combined system allowing the simultaneous phase imaging and Raman spectroscopy measurements [26]. OBJ1: fiber-coupling objective; OBJ2: microscope objective; YF: single wavelength optical fiber; C1, C2: beam collimators; A: attenuator; L1–L4: lenses; λ/2: half-plate; BS: beam splitter; LPF: long-pass filter; M1, M2: mirrors; DM: dichroic mirror; CCD1: CCD camera for holographic imaging; CCD2: CCD camera of the monochromator; BS45: 45° dichroic beam splitter; NF0: 0° notch filter; S: monochromator.

The combined system consists of a holographic set up as described in Section 2 utilizing a red coherent laser source, combined with a Raman microscope where the probe source was a separate diode laser (green source). The same objective lens used for the holographic imaging was also used to focalize the Raman probe on the sample and to collect the back-scattered light. The advantage offered by the holographic approach to numerically refocus the object under test is instrumental for the proposed combined approach. Indeed, in order to maximize the Raman signal, the Raman probe (green-laser) has to be focused on the specimen. However, due to chromatic aberration, the holographic image acquired by using the coherent red laser results out of its focal plane. By means of the refocusing algorithm, this problem can be overcome so that the Raman spectra and the holograms can be acquired simultaneously. **Figure 10(a)** represents the reconstructed amplitude map at the acquisition plane obtained by in a single-shot measurement, out of its focal plane, of the investigated spermatozoon. Then, the amplitude map in **Figure 10(b)** was numerically processed by using the refocusing algorithm [26], providing the focused amplitude map of the propagated object field reported in **Figure 10(b)**. A pseudo 3D representation of this phase map is reported in **Figure 10(c)**.

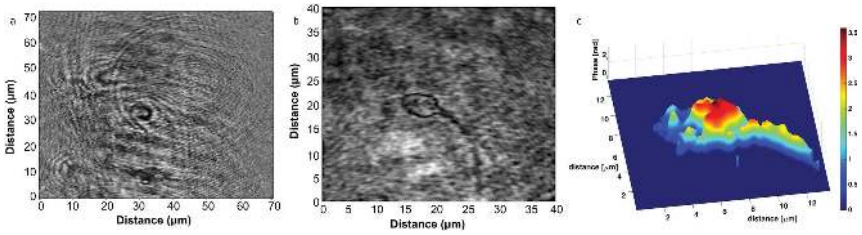

Figure 10. (a) Reconstructed amplitude map at the plane of acquisition; (b) Reconstructed amplitude map of the region of interest at the focus plane; (c) Pseudo 3D representation of the phase map of the region of interest at the focal plane. Ref. [26] (by permission of IEEE Society).

By using this combined approach, the effect of the green-laser light (Raman probe) by irradiating a specific region of the sperm cell was investigated for an increasing laser power from 4.4 to 50 mW, corresponding to the fluences in the range of 13–165 MJ/cm^2. The postacrosomal sperm cell region was irradiated for 3 s, and after each exposure, a single hologram and a Raman spectrum were simultaneously acquired. Raman measurements were performed using a green-laser power of 0.5 mW on the sample and an integration time of 20 s (green-light fluence of 10 MJ/cm^2); while, the red-light used for holographic measurements was set at 100 mW (red-light fluence of 100 mJ/cm^2). For the selected experimental conditions, any possible degradation effect associated with the red-laser light can be neglected [46]. Indeed, no adverse effects on the cells were observed even after hours of irradiation with red-laser light [47]. The biochemical characterization highlighted that the Raman bands related to localized vibration of the DNA bases (700–800 cm^{-1}) remains almost invariant when irradiated by the green-laser light, while the Raman bands associated with O-P-O (Oxygen-Phosphorus-Oxygen) backbone (900–1100 cm^{-1}) are subjected to photoinduced oxidation [47] and the peak at 1095 cm^{-1} decreases in intensity proportionally to the break of the double-helical structure with the fluences increase [48]. More precisely, it was observed that intensity decreases already after 30 MJ/cm^2 when no morphological changes were detected. In the spectral range of 1200–1400 cm^{-1}, the observed reduction in intensity of the peaks is at 1250 and 1375 cm^{-1}, already for fluence of 30 MJ/cm^2 was due to possible alterations in the secondary and tertiary conformation of proteins. Finally, all native nucleic acids exhibiting a broad and intense band near 1668 cm^{-1}, which originates from coupled C=O stretching and N–H deformation modes, are highly sensitive to disruption of Watson-Crick hydrogen bonding [47, 49]. At fluences higher than 150 MJ/cm^2, the spermatozoon is completely disintegrated [26]. Regarding the simultaneous morphological analysis, **Figure 11** shows the phase profile variations associated with the irradiating fluences, along the line SS′ (**Figure 11(b)**) and PP′ (**Figure 11(c)**), representing two different directions along the spermatozoa structure

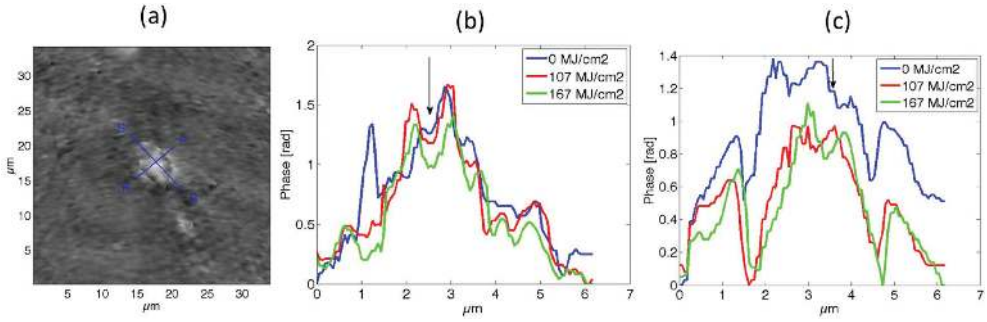

Figure 11. (a) Reconstructed phase map of the region of interest at the focus plane; the lines along which the profile is monitored during the exposition are highlighted. The Raman spectrum is acquired in the postacrosomal region. (b) Phase profile of the irradiated sperm cell at three different selected laser fluences along the lines SS′ and (c) PP′. Ref. [26] (by permission of IEEE Society).

(**Figure 11(a)**). The arrows indicate the regions of the sperm cells where the most relevant morphological variations were observed.

In **Figure 11(b)** and **(c)** a progressive reduction in the height, and therefore in the volume, is well visible, suggesting a sort of "photoporation" near the exposed region. At fluences higher than 150 MJ/cm^2, the sperm cell seemed to swell and an increase of the luminescence background of the Raman signal was observed confirming a local heating of the sample [47] due to the absorption at 532 nm [50–53].

6. Conclusion

In this chapter, an overview of the recent achievements in holography imaging applied to both morphological and motility characterizations of sperm cells has been reported. Results obtained by means of digital holography have demonstrated the possibility to provide 3D information on both the morphology and motility of sperm cells; this information could be used to better emphasize the differences between normal and abnormal sperm morphology. Moreover, the DH approach is a noninvasive technique, allowing the analysis of live spermatozoa, such as 3D tracking of the spatial motion, in order to select normal sperm cells. In particular, the possibility offered by digital holography to add the third dimension in the sperm analysis will give information useful both to relate the sperm anomalies with male infertility and to enable differentiation of the spermatozoa in good health. Finally, DH can be easily combined with other techniques allowing different simultaneous characterization. Indeed, it was demonstrated that a promising optical approach, based on digital holography and Raman spectroscopy technologies can be used for the quality assessment of spermatozoa. Applying this combined approach for analyzing the sperm cells, high-resolution images, and Raman spectra have been obtained, clearly highlighting some morphological and biochemical alterations. In particular, DH and Raman spectroscopy simultaneous approach was used for studying the photodamage induced by visible green light in the spermatozoa structure.

Author details

Giuseppe Coppola[1]*, Maria Antonietta Ferrara[1], Giuseppe Di Caprio[2], Gianfranco Coppola[3] and Brian Dale[3]

*Address all correspondence to: giuseppe.coppola@cnr.it

1 Institute for Microelectronics and Microsystems, National Research Council, Naples, Italy

2 Cell Biology Department at Harvard Medical School, Boston, MA, USA

3 Centre of Assisted Fertilization (CFA-Italy), Naples, Italy

References

[1] P.C. Steptoe, R.G. Edwards. Birth after the reimplantation of a human embryo. Lancet. 1978;12:366.

[2] M.J. Allen, E.M. Bradbury, R. Balhorn. The natural subcellular surface structure of the bovine sperm cell. J. Struct. Biol.. 1995;114(3):197–208.

[3] N. Cassuto, A. Hazout, I. Hammoud, R. Balet, D. Bouret, Y. Barak, S. Jellad, J.M. Plouchart, J. Selva, C. Yazbeckd. Correlation between DNA defect and sperm-head morphology. Reprod. Biomed. Online. 2012;24(12):211–218.

[4] T.G. Cooper, E. Noonan, S. von Eckardstein, J. Auger, H.W. Baker, H.M. Behre, T.B. Haugen, T. Kruger, C. Wang, M.T. Mbizvo, K.M. Vogelsong. World Health Organization reference values for human semen characteristics: Update. Hum. Reprod. 2010;16(3) 231-245. DOI: 10.1093/humupd/dmp048

[5] R.D. Franken. The clinical significance of sperm-zona pellucida binding. Front. Biosci. 1998;3:247–253.

[6] J. Parinaud, G. Vieitez, H. Moutaffian, G. Richoilley, P. Milhet. Relationships between motility parameters, morphology and acrosomal status of human spermatozoa. Hum. Reprod. 1996;11(6):1240–1243.

[7] J. Auger, F. Eustache, A.G. Andersen, D.S. Irvine, N. Jorgensen, N.E. Skakkebaek, J. Suominen, J. Toppari, M. Vierula, P. Jouannet. Sperm morphological defects related to environment, lifestyle and medical history of 1001 male partners of pregnant women from four European cities. Hum. Reprod. 2001;16(12):2710–2717.

[8] T.F. Kruger, A.A. Acosta, K.F. Simmons, R.J. Swanson, J.F. Matta, S. Oehninger. Predictive value of abnormal sperm morphology in in vitro fertilization. Fertil. Steril. 1988;49:112–117.

[9] B. Bartoov, A. Berkovitz, F. Eltes, A. Kogosowski, Y. Menezo, Y. Barak. Real-time fine morphology of motile human sperm cells is associated with IVF-ICSI outcome. J. Androl. 2002;23:1–8.

[10] B. Bartoov, F. Eltes, M. Pansky, H. Lederman, E. Caspi, and Y. Soffer. Estimating fertility potential via semen analysis data. Hum. Reprod. 1993;8:65–70.

[11] R. Mashiach, B. Fisch, F. Eltes, Y. Tadir, J. Ovadia, and B. Bartoov. The relationship between sperm ultrastructural features and fertilizing capacity in vitro. Fertil. Steril. 1992;57:1052–1057.

[12] R.J. Pieper, A. Korpel. Image processing for extended depth of field. Appl. Opt. 1983;22:1449–1453. DOI: 10.1364/AO.22.001449

[13] M.K. Kim, editor. Digital Holographic Microscopy: Principles, Techniques and Applications. Berlin: Springer; 2011.

[14] L. Yaroslavsky, editor. Digital Holography and Digital Image Processing: Principles, Methods, Algorithms. Philadelphia: Kluwer; 2004.

[15] G. Popescu, editor. Quantitative Phase Imaging of Cells and Tissues. New York: McGraw-Hill Professional; 2011.

[16] N. Shaked, Z. Zalevsky, L.L. Satterwhite, editor. Biomedical Optical Phase Microscopy and Nanoscopy. Amsterdam: Elsevier; 2012.

[17] U. Schanrs, W. Juptner. Direct recording of holograms by a CCD target and numerical reconstruction. Appl. Opt. 1994;33(2):179–181. DOI: 10.1364/AO.33.000179

[18] G. Di Caprio, M.A. Ferrara, L. Miccio, F. Merola, P. Memmolo, P. Ferraro, G. Coppola. Holographic imaging of unlabeled sperm cells for semen analysis: A review. J. Biophotonics. 2014;8(10):779–789. DOI: 10.1002/jbio.201400093

[19] W.S. Ward. Function of sperm chromatin structural elements in fertilization and development. Mol. Hum. Reprod. 2010;16(1):30–36. DOI: 10.1093/molehr/gap080

[20] L. Bernardini, A. Borini, S. Preti, N. Conte, C. Flamigni, G.L. Capitanio, P.L. Venturini. Study of aneuploidy in normal and abnormal germ cells from semen of fertile and infertile men. Hum. Reprod. 1998;13(12):3406–3413.

[21] L. Robinson, I.D. Gallos, S.J. Conner, M. Rajkhowa, D. Miller, S. Lewis, J. Kirkman-Brown, A. Coomarasamy. The effect of sperm DNA fragmentation on miscarriage rates: A systematic review and meta-analysis. Hum. Reprod. 2012;27(10):2908–2917, (2012). DOI: 10.1093/humrep/des261

[22] V. Sánchez, J. Wistuba, C. Mallidis. Semen analysis: Update on clinical value, current needs and future perspectives. Reproduction. 2013;146(6):R249–R258. DOI: 10.1530/REP-13-0109

[23] J.L. Fernandez, L. Muriel, V. Goyanes, E. Segrelles, J. Gosalvez, M. Enciso, M. LaFromboise, C. De Jonge. Simple determination of human sperm DNA fragmentation with an improved sperm chromatin dispersion test. Fertil. Steril. 2005;84:833–842. DOI: 10.1016/j.fertnstert.2004.11.089

[24] A. Giwercman, L. Lindstedt, M. Larsson, M. Bungum, M. Spano, R.J. Levine, L. Rylander. Sperm chromatin structure assay as an independent predictor of fertility in vivo: A case-control study. Int. J. Androl. 2010;33(1):e221–e227. DOI: 10.1111/j.1365-2605.2009.00995.x

[25] R. Henkel, E. Kierspel, M. Hajimohammad, T. Stalf, C. Hoogendijk, C. Mehnert, R. Menkveld, W.B. Schill, T.F. Kruger. DNA fragmentation of spermatozoa and assisted reproduction technology. Reprod. Biomed. Online. 2003;7(4):477–484.

[26] M.A. Ferrara, A. De Angelis, A.C. De Luca, G. Coppola, B. Dale, G. Coppola. Simultaneous holographic microscopy and Raman spectroscopy monitoring of human spermatozoa photodegradation. IEEE J. Sel. Top. Quantum Electron. 2015;22(3):5200108 DOI 10.1109/JSTQE.2015.2496265

[27] M. Montag, editor. A Practical Guide to Selecting Gametes and Embryos. CRC Press, Taylor & Francis Group - Boca Raton, FL (USA); 2014.

[28] Y. Takaki, H. Kawai, H. Ohzu. Hybrid holographic microscopy free of conjugate and zero-order images. Appl. Opt. 1999;38(23):4990–4996. DOI: 10.1364/AO.38.004990

[29] W. Hu, M.H. Jericho, I.A. Meinertzhagen, H.J. Kreuzer. Digital in-line holography for biological applications. Proc. Natl. Acad. Sci. U. S. A. 2001;98(20):11301–11305. DOI: 10.1073/pnas.191361398

[30] G. Pedrini, S. Schedin, H.J. Tiziani. Aberration compensation in digital holographic reconstruction of microscopic objects. J. Mod. Opt. 2001;48:1035–1041.

[31] S. De Nicola, P. Ferraro, A. Finizio, G. Pierattini. Wave front reconstruction of Fresnel off-axis holograms with compensation of aberrations by means of phase-shifting digital holography. Opt. Laser Eng. 2002;37:974–976.

[32] P. Ferraro, S. De Nicola, A. Finizio, G. Coppola, S. Grilli, C. Magro, and G. Pierattini. Compensation of the inherent wave front curvature in digital holographic coherent microscopy for quantitative phase-contrast imaging. Appl. Opt. 2003;42:1938–1946.

[33] G. Di Caprio, M. Gioffré, N. Saffioti, S. Grilli, P. Ferraro, R. Puglisi, D. Balduzzi, A. Galli, G. Coppola. Quantitative label-free animal sperm imaging by means of digital holographic microscopy. IEEE J. Quantum Electron. 2010;16(4):833–840.

[34] E.S.E. Hafez, editor. Reproduction in Farm Animals. Philadelphia: Lea & Febiger; 1987.

[35] I. Crha, J. Zakova, M. Huser, P. Ventruba, E. Lousova, M. Pohanka. Digital holographic microscopy in human sperm imaging. J. Assist. Reprod. Genet. 2011;28:725–729. DOI: 10.1007/s10815-011-9584-y

[36] G. Coppola, G. Di Caprio, M. Wilding, P. Ferraro, G. Esposito, L. Di Matteo, R. Dale, G. Coppola, B. Dale. Digital holographic microscopy for the evaluation of human sperm structure. Zygote. 2013. DOI: 10.1017/S0967199413000026

[37] P. Memmolo, G. Di Caprio, C. Distante, M. Paturzo, R. Puglisi, D. Balduzzi, A. Galli, G. Coppola, P. Ferraro. Identification of bovine sperm head for morphometry analysis in quantitative phase-contrast holographic microscopy. Opt. Exp. 2011;19(23):23215–23226. DOI: 10.1364/OE.19.023215

[38] F.C. Cheong, B.S.R. Dreyfus, J. Amato-Grill, K. Xiao, L. Dixon, D.G. Grierin. Flow visualization and flow cytometry with holographic video microscopy. Opt. Exp. 2009;17(15): 13071–13079. DOI: 10.1364/OE.17.013071

[39] S.T. Mortimer. CASA—Practical aspects. J. Androl. 2000;21(4):515–524.

[40] A. Guerrero, J. Carneiro, A. Pimentel, C.D. Wood, G. Corkidi, A. Darszon. Strategies for locating the female gamete: The importance of measuring sperm trajectories in three spatial dimensions. Mol. Hum. Reprod. 2011;17(8):511–523. DOI: 10.1093/molehr/gar042

[41] T.-W. Su, L. Xue, A. Ozcan. High-throughput lensfree 3D tracking of human sperms reveals rare statistics of helical trajectories. Proc. Natl. Acad. Sci. USA. 2012;109(40):16018–16022. DOI: 10.1073/pnas.1212506109

[42] G. Di Caprio, A. El Mallahi, P. Ferraro, R. Dale, G. Coppola, B. Dale, G. Coppola, F. Dubois. 4D tracking of clinical seminal samples for quantitative characterization of motility parameters. Biomed. Opt. Express. 2014;5(3):690–700. DOI: 10.1364/BOE.5.000690

[43] G.E. Forsythe, M.A. Malcolm, C.B. Moler, editors. Computer Methods for Mathematical Computations. Upper Saddle River, NJ: Prentice-Hall; 1976.

[44] G. Di Caprio, A. El Mallahi, P. Ferraro, G. Coppola, F. Dubois. Automatic algorithm for the detection and 3D tracking of biological particles in digital holographic microscopy. In: Proceedings EOS: Topical Meeting on Optical Microsystems. Capri—Italy: European Optical Society; 2011.

[45] A. El Mallahi, C. Minetti, F. Dubois. Automated three-dimensional detection and classification of living organisms using digital holographic microscopy with partial spatial coherent source: Application to the monitoring of drinking water resources. Appl. Opt. 2013;52(1):A68–A80. DOI: 10.1364/AO.52.000A68

[46] G.J. Puppels, J.H. Olminkhof, G.M.J. Segers-Nolten, C. Otto, F.F.M. De Mul, J. Greeve. Laser irradiation and Raman spectroscopy of single living cells and chromosomes: Sample degradation occurs with 514.5 nm but not with 660 nm laser light. Exp. Cell Res. 1991;195:361–367. DOI:10.1016/0014-4827(91)90385-8.

[47] H. Barry, I.A. Okezie, editor. DNA and Free Radicals. England: Ellis Horwood Limited; 1993.

[48] J.M. Benevides, P.L. Stow, L.L. Ilag, N.L. Incardona, G.J. Thomas. Differences in secondary structure between packaged and unpackaged single-stranded DNA of bacteriophage φX174 determined by Raman spectroscopy: A model for φX174 DNA packaging. Biochemistry. 1991;30(20):4855–4863.

[49] L. Lafleur, J. Rice, G.J. Thomas. Raman studies of nucleic acids. VII. Poly(A) * poly(U) and poly(G) * poly(C). Biopolymers. 1972;11:2423–2437.

[50] S. Milutin. Detection of semen and blood stains using polilight as a light source. Forens. Sci. Int.. 1991;51:289–296.

[51] Y. Liu, D.K. Cheng, G.J. Sonek, M.W. Berns, C.F. Chapman, B.J. Tromberg. Evidence for localized cell heating induced by infrared optical tweezer. J. Biophys. 1995;68:2137–2144.

[52] Y. Liu, G.J. Sonek, M.W. Berns, B.J. Tromberg. Physiological monitoring of optically trapped cells: Assessing the effects of confinement by 1064 laser tweezers using microfluorometry. J. Biophys. 1996;71:2158–2167.

[53] E.J.G. Peterman, F. Gittes, C.F. Schmidt. Laser induced heating in optical traps. J. Biophys. 2003;84:1308–1316.